Electronic Supplementary Information (ESI)

Hydrophilic Janus-faced Separator with Functionalized Nanocarbon for Stable Cycling of Aqueous Zn-metal Batteries

Hyuntae Lee[‡,a], Jiwoong Kang[‡,a], Ho Won Kang[b], Mingyu Lee[a], Jaewoong Han[a], Minhong Lim[a], Jaeho Lee[a], Woosuck Kwon[a], Dae-Hyun Nam[a,c], Byung Gon Kim[b,*] and Hongkyung Lee[a,c,*]

[a]Department of Energy Science & Engineering, Daegu Gyeongbuk Institute of Science and Technology (DGIST), 333 Technojungang-daero, Hyeonpung-Eup, Dalseong-gun, Daegu 42988, Republic of Korea

[b]Department of Applied Chemistry, Kyung Hee University, 1732 Deogyeong-daero, Giheung-gu, Yongin-si, Gyeonggi-do 17104, Republic of Korea

[c]Energy Science & Engineering Center, DGIST, 333 Technojungang-daero, Hyeonpung-Eup, Dalseong-gun, Daegu 42988, Republic of Korea

[‡]These authors equally contributed to this work.

* Emails: hongkyung.lee@dgist.ac.kr (H.L.); byunggonkim@khu.ac.kr (B.G.K.)

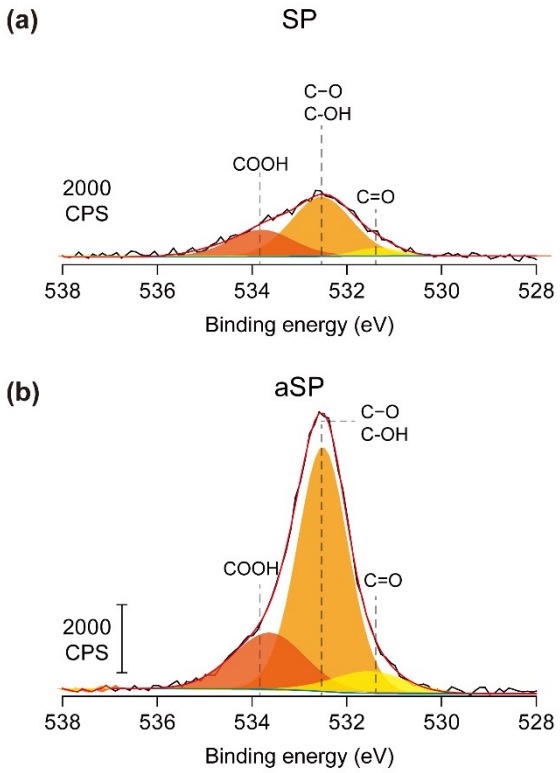

Fig. S1. Deconvoluted high-resolution XPS spectra of O 1s (a) SP, and (b) aSP.

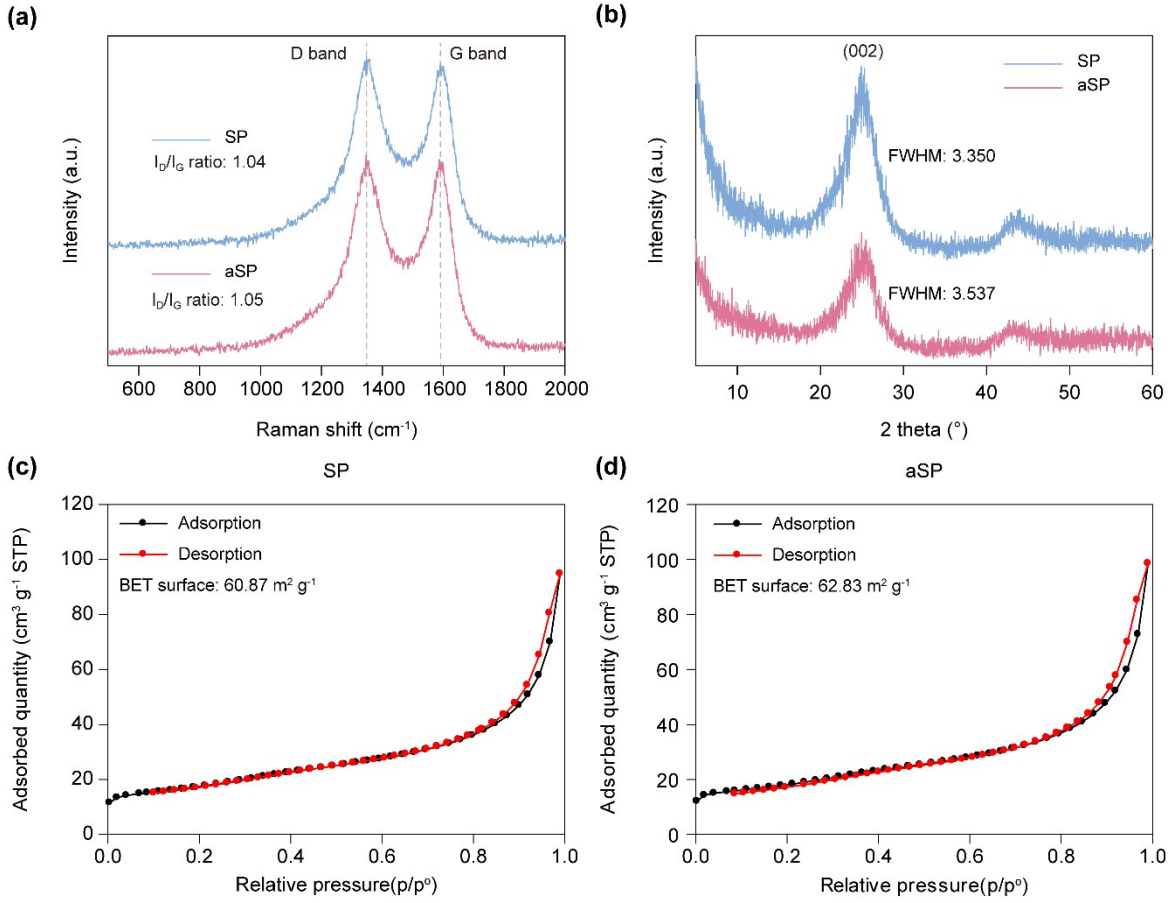

Fig. S2. The characterization of SP and aSP (a) Raman spectra, (b) XRD patterns, and N_2 adsorption-desorption isotherm curves of the (c) SP and (d) aSP. In Raman spectra, the ratio of peak intensities of the D band (disordered carbon) and G band (graphitic carbon) (I_D/I_G) for the aSP (1.05) showed negligible differences from that of the SP (1.04). Moreover, the full width at half-maximum (FWHM) values for aSP (2θ=3.537°) and SP (2θ=3.350°) were closely comparable at the XRD peak. Accordingly, the aSP and SP showed minimal differences in BET surface area. This series of analytical results reveals that the acid treatment has negligible impact on the bulk domain of carbon and mainly contributes to the formation of functional groups on carbon surface.

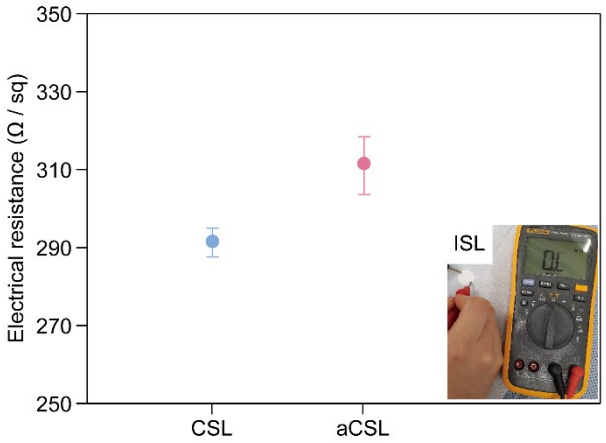

Fig. S3. The 4-point-probe measurement result for CSL and aCSL. In set optical image is the measurement of electrical resistance for ISL by multi-meter.

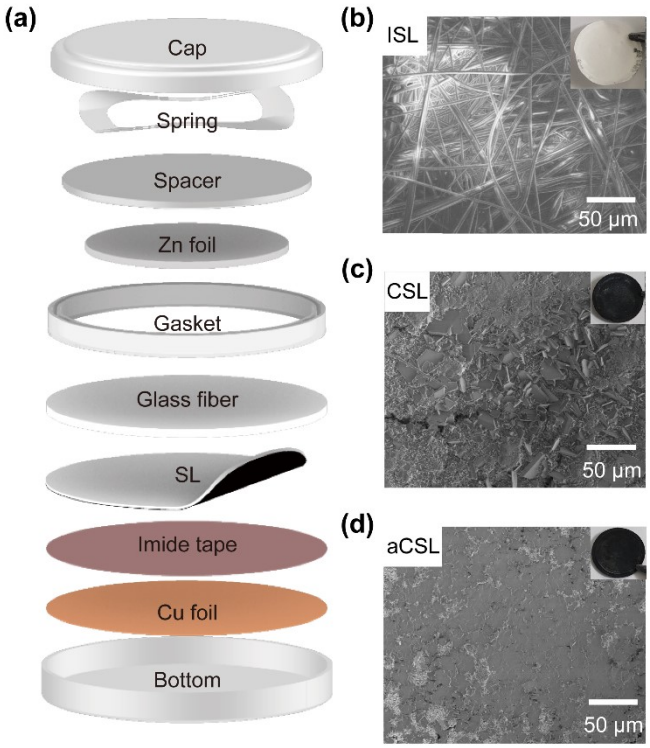

Fig. S4. (a) The cell configuration of Zn||Cu cell which Cu is insulated by imide tape, and the Zn deposition SEM images of (b) ISL, (c) CSL, and (d) aCSL at 1 mA cm^{-2} and 1 mAh cm^{-2}.

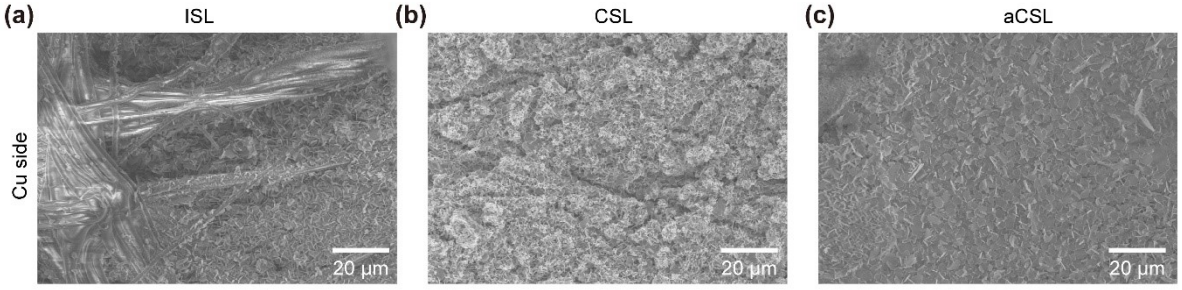

Fig. S5. The SEM image of Zn deposition at Zn||Cu asymmetric cell at 1 mA cm^{-2} and 5 mAh cm^{-2} (a) ISL, (b) CSL, and (c) aCSL.

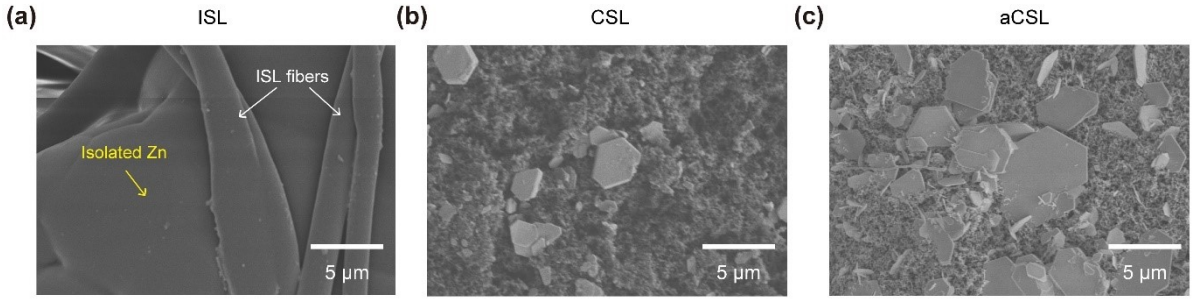

Fig. S6. The high-magnified SEM image of separator side of (a) ISL, (b) CSL, and (c) aCSL cells shown in Fig. 2a-c, after Zn deposition at 1 mA cm^{-2} and 5 mAh cm^{-2}.

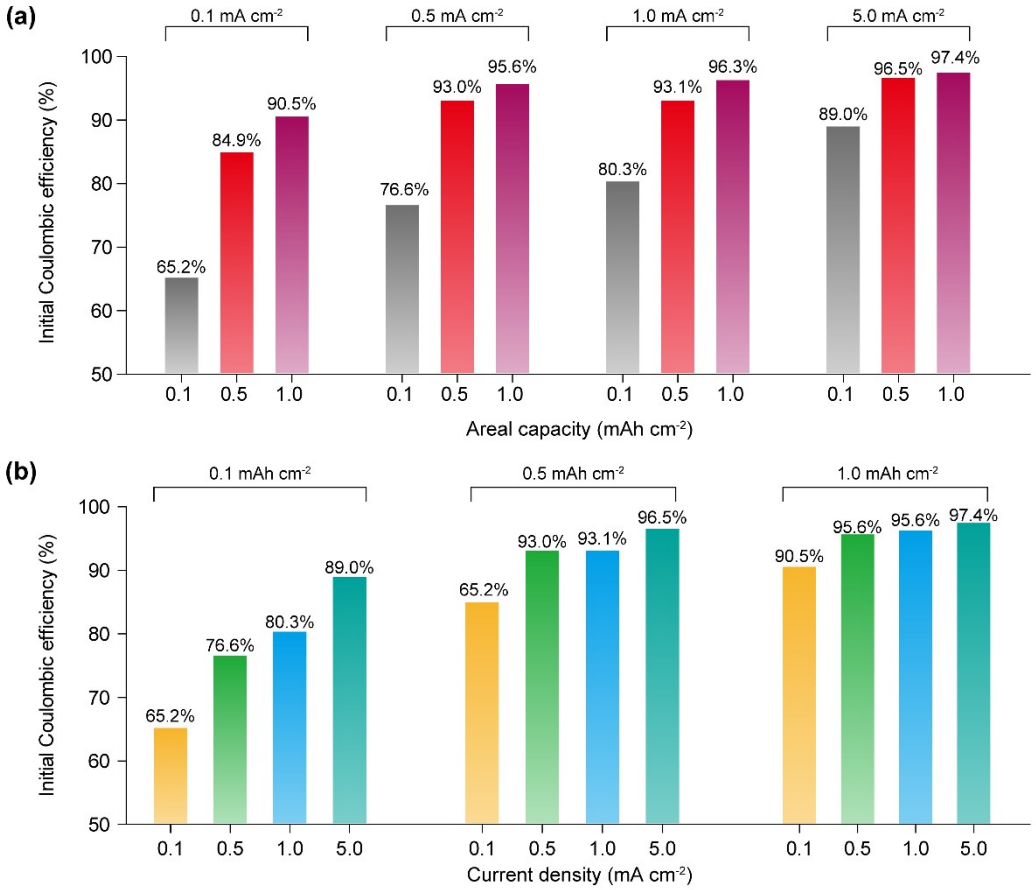

Fig. S7. The initial Coulombic efficiency of Zn||Cu asymmetric cell at various (a) current densities and (b) Zn plating capacity (areal capacity).

Fig. S7 presents the results of ICE measurements under different current densities and Zn plating capacities. The ICE values exhibited an increasing trend as the current densities were raised while keeping the Zn plating capacity constant. Similarly, the ICE values increased when the Zn plating capacity was enhanced while maintaining a fixed current density.

This observation suggests that the HER is effectively suppressed by higher current densities, leading to an increase in the ICE of Zn. Conversely, the ICE values also exhibited an upward trend as the Zn deposition capacity was augmented under fixed current density conditions. This finding implies that the corrosion products of ZMA could be maintained, and an increased Zn deposition capacity can positively impact the ICE performance.

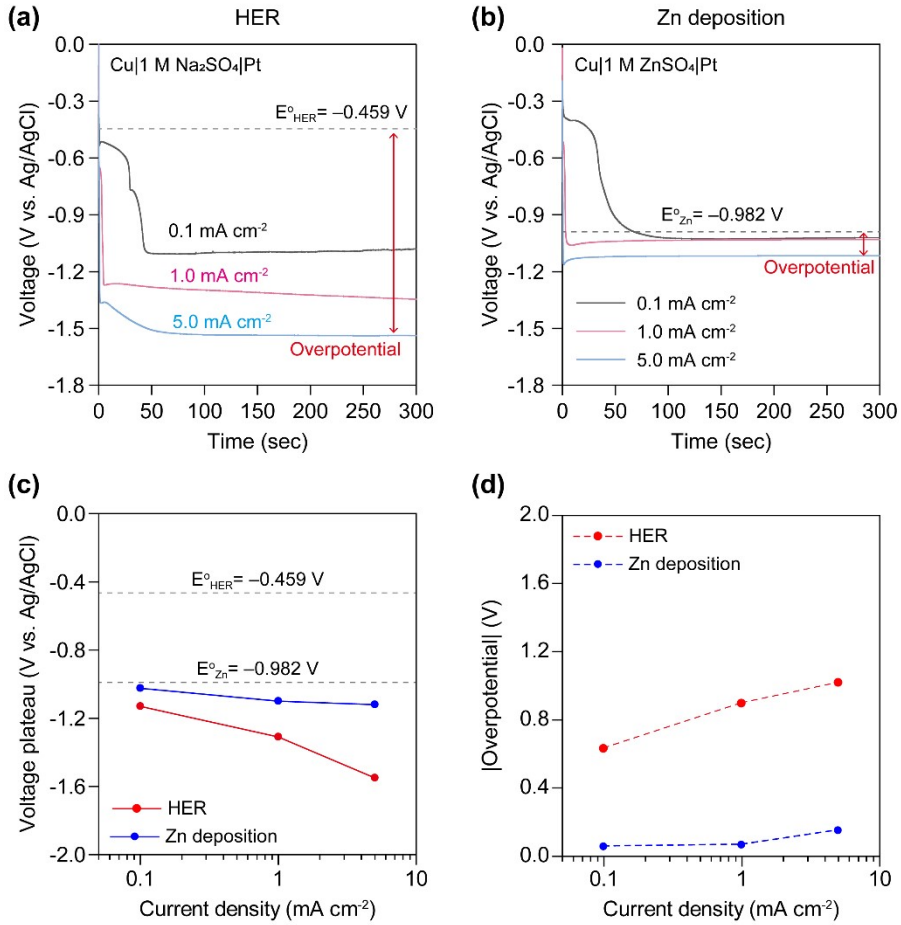

Fig. S8. Chronopotentiometry curves at various current densities showing the voltage plateau for (a) HER and (b) Zn deposition. Comparison of the (c) voltage plateau and (d) overpotentials between HER and Zn deposition.

To calculate overpotential, determining the equilibrium potentials of HER (E_{HER}) and Zn deposition (E_{Zn}) in a 2 M $ZnSO_4$ electrolyte (pH 4) is essential, using the Nernst equation:

$$E_{Zn} = E_{Zn}^{\circ} - \frac{RT}{nF}\ln\frac{1}{a_{Zn^{2+}}}, \quad E_{HER} = E_{HER}^{\circ} - \frac{RT}{nF}\ln\frac{1}{a_{H^{+}}^{2}}$$

, where n is the number of electrons (2), F is the Faraday constant, R is the universal gas constant, $a_{Zn^{2+}}$ and $a_{H^{+}}$ represent the activities Zn^{2+} and H^{+}, respectively. The E_{Zn} and E_{HER} were calculated to –0.982 V vs. Ag/AgCl (–0.751 V vs. SHE) and –0.459 V vs. Ag/AgCl (–0.237 V vs. SHE), respectively. To assess polarization in HER and Zn electroplating reactions, voltage plateaus at 0.1, 1.0, and 5.0 mA cm^{-2} were measured using chronopotentiometry in a three-electrode cell (Cu working electrode, Pt counter electrode, and Ag/AgCl reference electrode) with 1 M Na_2SO_4 and 1 M $ZnSO_4$ electrolytes (pH 4) for reaction separation. Overpotentials were determined by the difference between the voltage plateau and their respective equilibrium potentials.

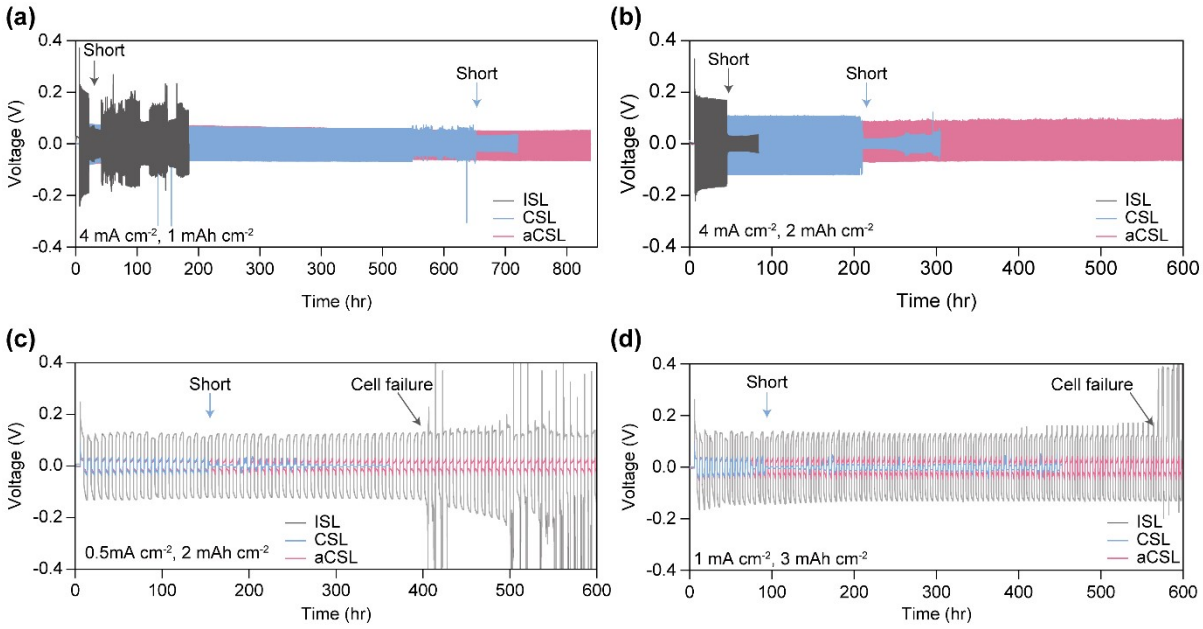

Fig. S9. Voltage profiles of Zn||Zn symmetric cells integrated with the ISL, CSL, and aCSL at various current densities and Zn plating capacities: (a) 4 mA cm^{-2} and 1 mAh cm^{-2}, (b) 4 mA cm^{-2} and 2 mAh cm^{-2}, (c) 0.5 mA cm^{-2} and 2 mAh cm^{-2}, and (d) 1 mA cm^{-2} and 3 mAh cm^{-2}, respectively.

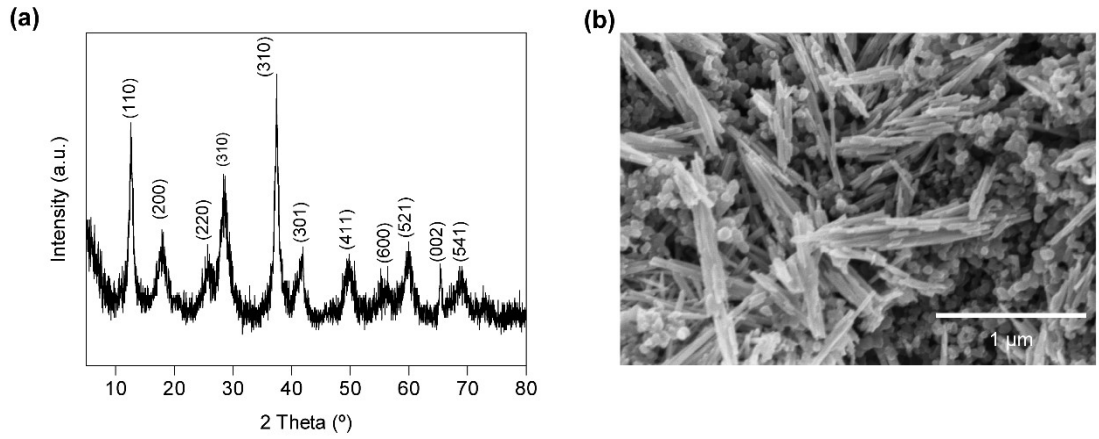

Fig. S10. The analysis of synthesized α-MnO_2/CNT cathode (a) XRD analysis, and (b) SEM image.

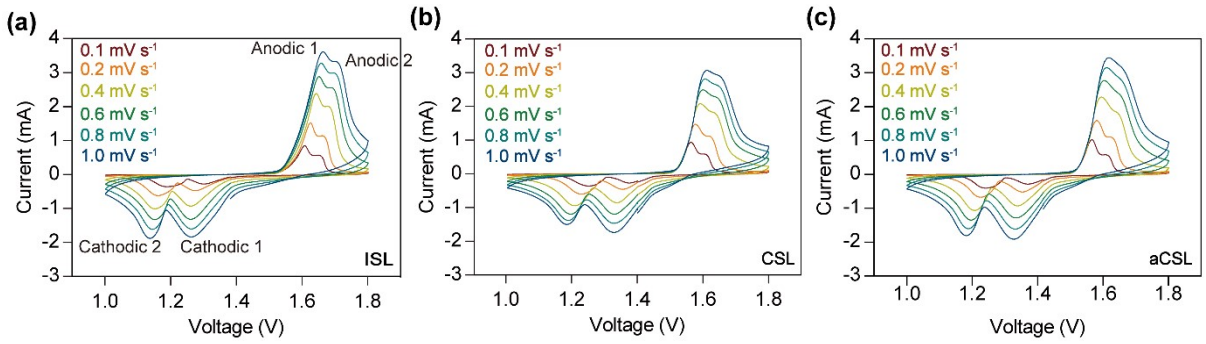

Fig. S11. CV profiles of the Zn||α-MnO_2/CNT full cells with various scan rates (a) ISL, (b) CSL, and (c) aCSL.

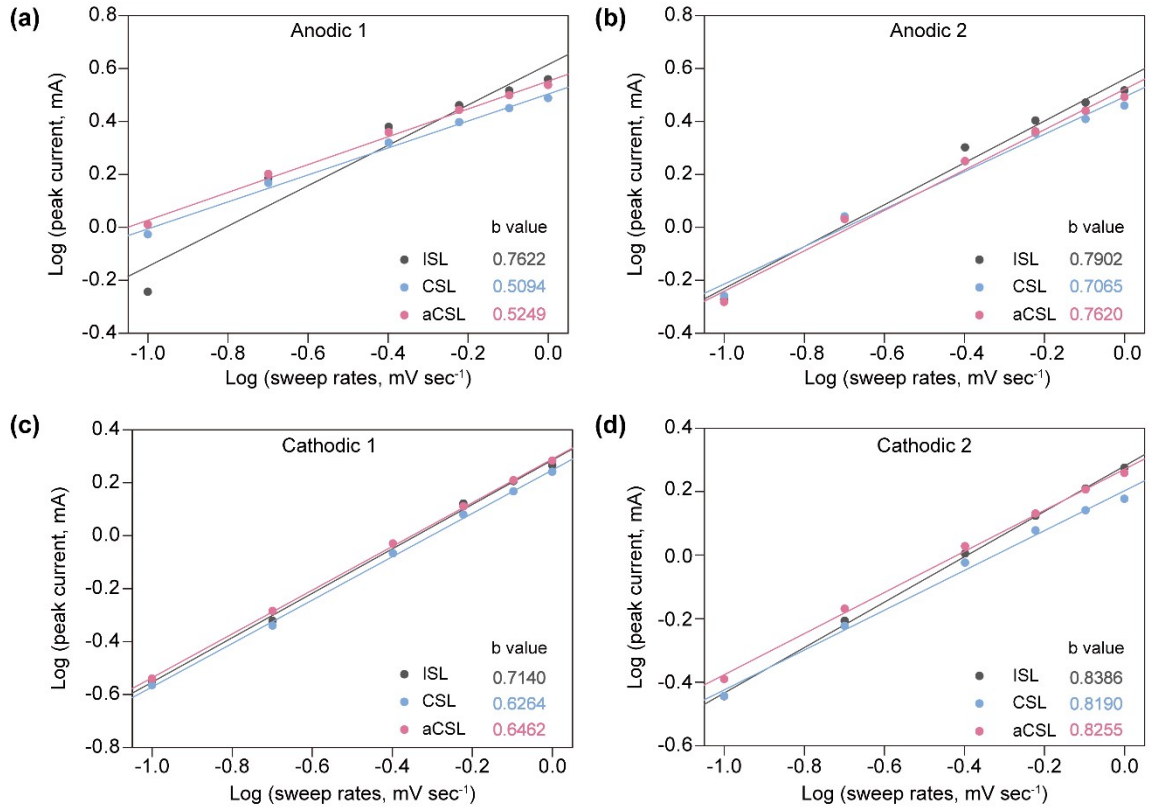

Fig. S12. The relationship between the CV peak current and scan rate in a logarithmic form of Zn||α-MnO_2/CNT full cells for each SL (a) Anodic 1, (b) Anodic 2, (c) Cathodic 1, and (d) Cathodic 2.

CV measurements were performed at different scan rates to identify the charge storage mechanism. The relationship between the peak current (i) and scan rate (v) is described by the power law[1-3]:

$$i = av^b \text{ (Equation S1)}$$

The exponent b is indicative of the charge storage mechanism. The calculated b values of aCSL exhibited all four anodic and cathodic peaks (0.53, 0.76, 0.65, 0.83 is indicating anodic 1, anodic 2, cathodic 1, and cathodic 2, respectively) were shown higher than CSL (0.51, 0.71, 0.63, 0.82 is indicating anodic 1, anodic 2, cathodic 1, and cathodic 2, respectively). This indicates that the charge storage mechanism of Zn||α-MnO_2 cells with SLs is based on more capacitive chare storage process and aCSL shows enhanced charge storage speed than CSL due to its large active surface.

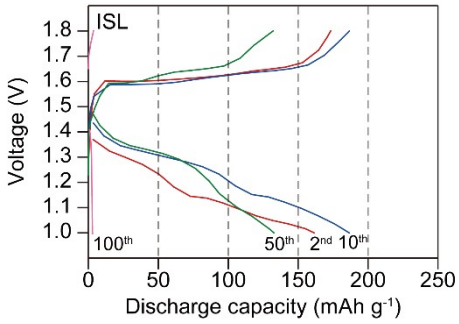

Fig. S13. The voltage profile of Zn||α-MnO_2/CNT full cell with ISL for long-term cycling.

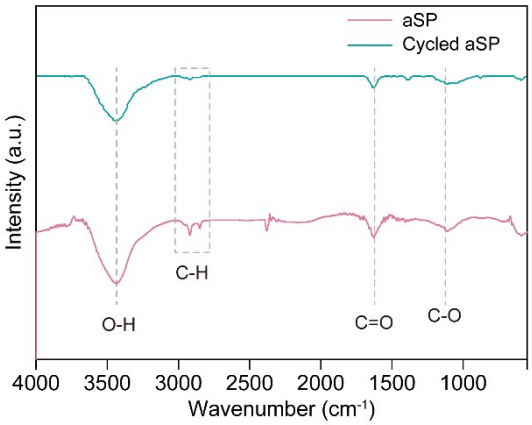

Fig. S14. FT-IR analysis of aSP particles before and after 100 cycles in the Zn||α-MnO_2/CNT full cell with aCSL, illustrating the stability of functional groups under cycling conditions.

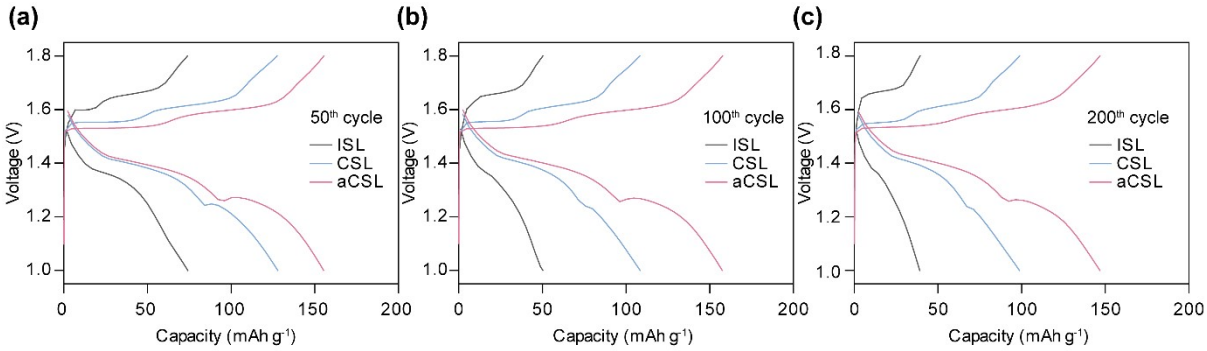

Fig. S15. The voltage profile of Zn||α-MnO_2/CNT full cells with high mass loading of ~ 2 mg cm^{-2} (a) 50th cycle, (b) 100th cycle, and (c) 200th cycle.

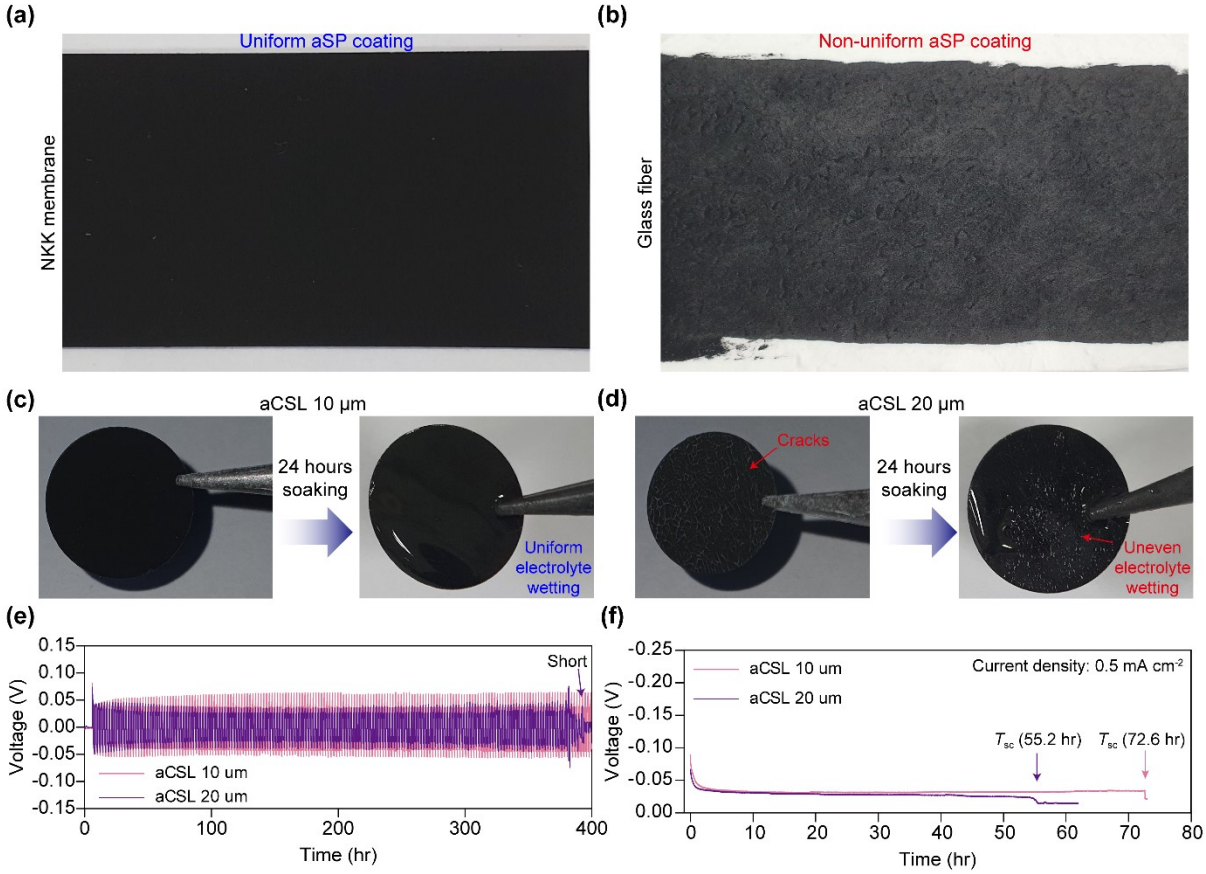

Fig. S16. The digital images of aCSL coating quality on two different substrates (a) NKK membrane and (b) glass fiber. Digital images of aCSL and aCSL soaked in 2 M $ZnSO_4$ electrolyte with different thickness. (c) 10 μm and (d) 20 μm-thick aCSL. Voltage profiles of Zn||Zn symmetric cells with 10 μm and 20 μm aCSL: (e) cycling at 1 mA cm^{-2}, 1 mAh cm^{-2}; (f) T_{sc} at 0.5 mA cm^{-2}.

Table S1. Summary of electrochemical results of previous Zn||Zn symmetric cells related to the separator modification approach.

Separator	Increased thickness (μm)	Current density (mA cm^{-2})	Cycling capacity (mAh cm^{-2})	Cycling life (hour)	Ref
PAN-S	30	0.5	1	350	[29]
VG-GF separator	Negligible	1	1	250	[34]
MXene-GF separator	Negligible	1	1	1200	[36]
MOF/rGO	25	2	1	500	[54]
SPAES@GF	10	1	1	2000	[55]
Cellulose/g-C_3N_4	70	3	1	590	[56]
Cellulose film	-	1	1	2000	[57]
CS@NGDY	170	5	1	500	[58]
aCSL	10	1	1	2400	This work
		4	1	800	

Supplementary references

1. H. Lindström, S. Södergren, A. Solbrand, H. Rensmo, J. Hjelm, A. Hagfeldt and S.-E. Lindquist, *J. Phys. Chem. B*, 1997, **101**, 7717-7722.
2. V. Augustyn, J. Come, M. A. Lowe, J. W. Kim, P.-L. Taberna, S. H. Tolbert, H. D. Abruña, P. Simon and B. Dunn, *Nat. Mater.*, 2013, **12**, 518-522.
3. J. Ding, Z. Du, L. Gu, B. Li, L. Wang, S. Wang, Y. Gong and S. Yang, *Adv. Mater.*, 2018, **30**, 1800762.